Effects of the Bi-Maxwellian Plasma on Active Spacecraft Charging in GEO

Amy Haft[1] and Hanspeter Schaub[2]

***Abstract*—The electrostatic tractor has been proposed as a promising solution to dispose of defunct satellites from Geosynchronous Earth Orbit (GEO). The electrostatic tractor concept postulates that a servicer spacecraft, which is equipped with an electron gun aimed at a target spacecraft, will use electron beam emissions to make the target electric potential negative while making its own potential positive. The resulting attractive electrostatic force is used to touchlessly pull the target into a graveyard orbit. Previous research has studied the effects of active spacecraft charging in an environment modeled using a single-Maxwellian distribution, but due to frequent geomagnetic substorms, the GEO environment is often better modeled by a bi-Maxwellian plasma where population 1 is the cooler core of electrons and ions and population 2 is the hot halo that is injected during a substorm. This paper studies natural charging due to the environment in a bi-Maxwellian plasma in addition to active charging in a bi-Maxwellian plasma. Results show that the electrostatic tractor would be most effective when the density of population 1 is significantly greater than the density of population 2. This is because as the density ratio population 1 to population 2 becomes large, the target equilibrium potential converges to a particular value. However, when the density ratio is small, perturbations in the environment can cause the target potential to jump between thousands of Volts.**

***Index Terms*—spacecraft charging, bi-maxwellian, space environments, geosynchronous orbit**

I. Introduction

The significant value of satellites in Geosynchronous Earth Orbit (GEO) [1] and the increasing risk of collisions due to debris-related congestion [2], [3] highlights the necessity of Active Debris Removal in the GEO regime. However, spin rates of uncooperative debris in the neighborhood of GEO have been observed to reach many 10s deg/s [4], [5], making it very challenging to safely mechanically grapple with these tumbling debris objects without extensive detumbling operations [6]. The electrostatic tractor concept has been proposed as a contactless method of GEO debris remediation [7]. Here, a servicer spacecraft is equipped with an electron gun to make the electric potential of the target negative while making its own potential positive, thus creating an attractive Coulomb electrostatic force that the servicer uses to pull the target into a graveyard orbit. The Debye lengths, a measure of how far a charge's electrostatic effect persists, of several hundreds of meters in the GEO space environment ensure that potential shielding due to the ambient plasma is not a concern [8].

1: Graduate Research Assistant at the University of Colorado Boulder. E-mail: amy.haft@colorado.edu

2: Professor and Department Chair, Schaden Leadership Chair, Ann and H.J. Smead Department of Aerospace Engineering Sciences, Colorado Center for Astrodynamics Research. AAS Fellow, AIAA Fellow

Previous charging studies on the electrostatic tractor concept have modeled the GEO environment using a single-Maxwellian distribution [9], [10]. However, non-thermal particle distributions in the solar-wind and near-Earth space plasma have been confirmed by several interplanetary missions [11]–[15]. These suprathermal deviations from the Maxwellian velocity distribution function are expected to exist in any low-density plasma in the Universe [16], which includes the GEO environment. Geomagnetic substorms significantly modify the particle distribution in GEO. During a substorm, the GEO orbit is injected with a cloud of very hot plasma with densities on the order of $10^6 - 10^7$ m^{-3} and energies of $1 - 50$ keV [17]. This is compared to the environment during quiet conditions, in which the plasma density is on the order of 10^8 m^{-3} with an energy of 1 eV [17]. Because the plasma at GEO is rarified and collisionless, the sudden injection of high-energy plasma during substorms every few hours [18] makes the environment a mixture of two different plasmas. Due to the frequency of geomagnetic substorms in this regime, it is more accurate to use a bi-Maxwellian distribution function to model the plasma environment.

In this paper, the impacts of the bi-Maxwellian plasma on spacecraft charging using an electron beam are investigated. Active charging in the single-Maxwellian environment is reviewed in section II. The bi-Maxwellian environment is described and investigated in section III. Results from simulations including the electron beam are analyzed in section IV.

II. Discussion on Charging in the Single-Maxwellian Environment

The onset of spacecraft charging in a single-Maxwellian plasma is generally understood and has been modeled both theoretically [19], [20] and experimentally, including thorough data collected by Los Alamos National Laboratory satellites [21], [22]. The velocity distribution function for a Maxwellian plasma $f(E)$ is [23]

$$f(E) = n\left(\frac{m}{2\pi k_B T}\right)^{3/2} \exp\left(-\frac{E}{k_B T}\right) \tag{1}$$

where n is the electron density, T is the electron temperature, m is the electron mass, k_B is the Boltzmann constant, and E is the electron energy, $E = \frac{1}{2}mv^2$.

Models confirm the existence of a critical temperature T^* that dictates the onset of negative charging [20]–[22]. Suppose the existence of a spacecraft that is initially charged to a zero volt potential $\phi_0 = 0$ in a space plasma that is at the

threshold condition required for negative charging to occur. Neglecting the ion current, the current balance is between the incoming ambient electrons and the outgoing backscattered η and secondary electrons δ. The current balance equation is then

$$\int_0^\infty f(E)E\mathrm{d}E = \int_0^\infty f(E)E[\delta(E)+\eta(E)]\mathrm{d}E \quad (2)$$

which has the equivalent form

$$\frac{\int_0^\infty f(E)E[\delta(E)+\eta(E)]\mathrm{d}E}{\int_0^\infty f(E)E\mathrm{d}E} = 1 \quad (3)$$

Because n appears in $f(E)$ on both sides of 2, it cancels out and the threshold condition is proportional only to T because the other coefficients are constant. The form seen in 3 is the threshold condition and, for simplicity, will be written in the following shorthand notation [24]:

$$< \delta(E)+\eta(E) >= 1 \quad (4)$$

T^* can then be determined by solving the threshold condition using the material properties required by the Sanders and Inouye secondary electron formula [25]

$$\delta(E) = c[\exp(-E/a) - \exp(-E/b)] \quad (5)$$

and the Prokopenko and Laframboise backscattered electron formula [26]

$$\eta(E) = A - B\exp(-CE) \quad (6)$$

where $a = 4.3E_{\max}$, $b = 0.367E_{\max}$, and $c = 1.37\delta_{\max}$ and A, B, and C depend on the surface materials.

After substitution, the threshold condition simply becomes [23]

$$c\left[(1+k_BT^*/a)^{-2} - (1+k_BT^*/b)^{-2}\right] + A - B(1+Ck_BT^*)^{-2} = 1 \quad (7)$$

In this paper, the material used is silver due to its consistent material properties across sources [23], [27] and NASCAP documentation [28]. The material properties for silver are a = 3.44, b = 0.2936, c = 1.37, A = 0.39, B = 0.2890, and C = 0.6320.

Fig. 1 illustrates the charging threshold in a Maxwellian environment for silver, where the second temperature where $< \delta(E)+\eta(E) >= 1$ is T^*. It is helpful to note that each material will have its own value of T^* depending on material properties [23]. The graph shows how the averaged value $< \delta(E)+\eta(E) >$ from 4, which is the threshold condition curve, compares to the total electron yield $\delta+\eta$ and the individual yields of the secondary and backscattered electrons, δ and η respectively. The first temperature where $< \delta(E)+\eta(E) >= 1$ is the anti-critical temperature $T_A = 0.3$keV and the second temperature is the critical temperature $T^* = 1.2$keV.

Recent work on active spacecraft charging using an electron beam in a Maxwellian environment found the existence of multiple equilibrium values [9]. In other words, there exist

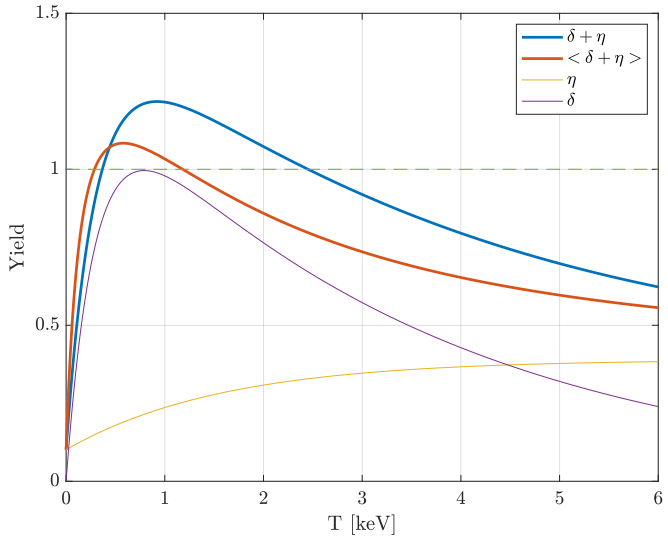

Fig. 1: Threshold plot for the material silver.

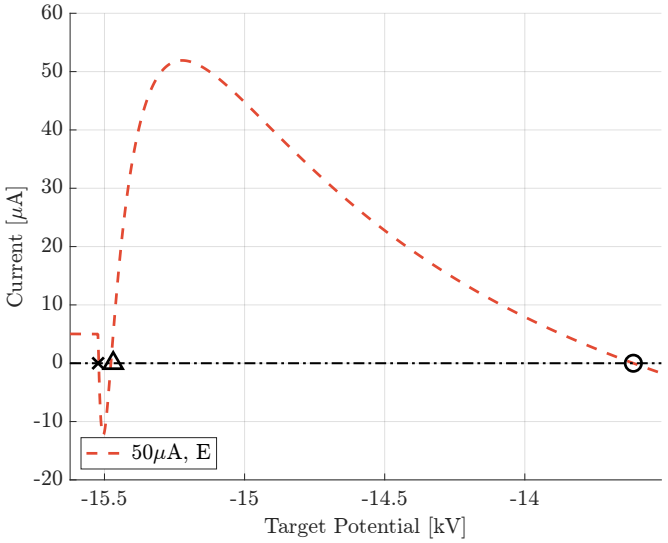

Fig. 2: Multiple equilibria in a Maxwellian environment [9].

multiple target object potentials where the net current on the target converges to zero. Fig. 2 illustrates how the the equilibrium values present themselves using an electron beam current of 50μA in an eclipse. Note that all results throughout this paper will present data for which the target object is eclipsed, meaning photoelectron emissions are neglected. The results from the study in [9] indicate that jumps between equilibria are possible due to changes in beam energy and environment.

III. The Bi-Maxwellian Space Environment

The multiple equilibria results from Ref. [9] perfectly allude to the theory of the potential jump, also known as the triple-root jump, in a bi-Maxwellian plasma. The triple-root jump theory states that it is possible to experience a sudden jump in spacecraft potential from a positive root of a few Volts to a negative root of thousands of volts while passing through an unstable third root. This concept was first proposed in 1965

[29] and confirmed experimentally in 1988 [30]. In summary, while it is possible for a spacecraft to experience multiple equilibrium potentials in a single-Maxwellian plasma with an electron beam current acting on it, a spacecraft may experience multiple equilibria naturally in a bi-Maxwellian plasma. In the discussion in this paper, the condition where $T_A < T_1 < T^* < T_2$ will be considered, where $T_{1,2}$ are the electron temperatures of population 1 and population 2. This is a common GEO space condition and the potential jumps that occur outside of this condition are not easily visualized.

The threshold condition for negative charging in a bi-Maxwellian space environment is significantly more complex than that for the single-Maxwellian environment. The derivation begins similarly: suppose an initially uncharged object $\phi_0 = 0$ in a space environment that is at the threshold condition where the ion contribution is neglected. The velocity distribution function for a bi-Maxwellian plasma is

$$f(E) = f_1(E) + f_2(E) \tag{8a}$$

$$f_1(E) = n_1 \left(\frac{m}{2\pi k_B T_1}\right)^{3/2} \exp\left(-\frac{E}{k_B T_1}\right) \tag{8b}$$

$$f_2(E) = n_2 \left(\frac{m}{2\pi k_B T_2}\right)^{3/2} \exp\left(-\frac{E}{k_B T_2}\right) \tag{8c}$$

where the subscripts 1 and 2 represent the respective values for electron population 1 and 2.

Then 2 can be transformed into

$$\int_0^\infty (f_1(E) + f_2(E)) E dE = \int_0^\infty (f_1(E) + f_2(E)) E[\delta(E) + \eta(E)] dE \tag{9}$$

which, after complex algebra and substituting in the required equations, becomes

$$\frac{\alpha(k_B T_1)^{1/2} < \delta(E) + \eta(E) >_1 + (k_B T_2)^{1/2} < \delta(E) + \eta(E) >_2}{\alpha(k_B T_1)^{1/2} + (k_B T_2)^{1/2}} = 1 \tag{10}$$

where $\alpha = n_1/n_2$. Ref. [24] shows this derivation in greater detail. This threshold condition for the case where $\phi_0 = 0$ will be denoted at threshold$_0$.

From 10, it is evident that the threshold condition in a bi-Maxwellian plasma is now dependent on 4 parameters: n_1, n_2, T_1, and T_2. For simplicity, α is used to combine n_1 and n_2 into a single parameter and reduce the number of independent variables to 3. As $\alpha \to \infty$, the plasma behaves like a single-Maxwellian plasma.

Fig. 3 gives an example of the threshold$_0$ condition for a fixed value of $T_2 = 2.1$keV. The U-shaped line corresponds to the threshold$_0$ condition. At a point (T_1, α) above the line within the shaded region, the spacecraft potential will converge to a few volts positive. Outside of the shaded region or below the U-shaped line, the spacecraft potential will converge to a negative value. Interestingly, the asymptotes of this threshold condition are at T_A and T^* corresponding to the material.

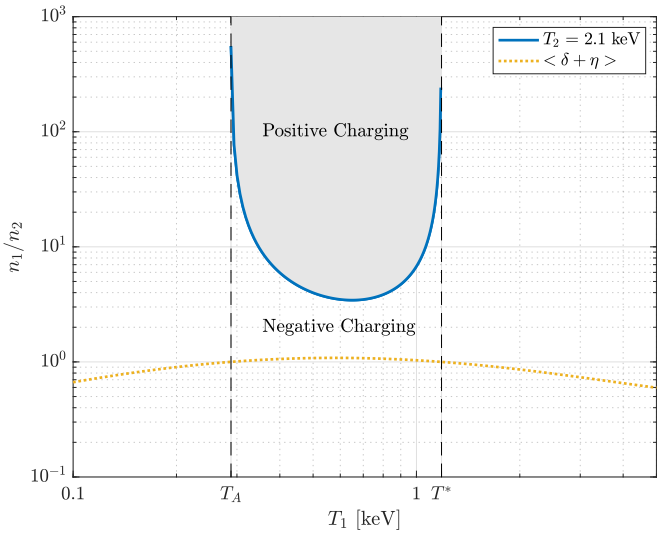

Fig. 3: Illustration of the threshold$_0$ condition for a fixed $T_2 = 2.1$keV.

Recall that the threshold$_0$ derivation does not account for the effect of ions in the space environment. The charging threshold in a more realistic space environment is easier to calculate numerically using a spacecraft charging model. The spacecraft charging model used in [9] is applied in this research. The model assumes a spherical, fully-conducting spacecraft such that all charging occurs on the surface and there is only one electric potential ϕ across the entire surface. The radii of the servicer and target spacecraft are set to $R_S = R_T = 1$m. The secondary and backscattered electron yields due to the incoming electron current are modeled by 5 and 6 for consistency across previous bi-Maxwellian research [23], [24], [31]. The other equations remain the same.

Fig. 4 illustrates the charging threshold for the natural environment in an eclipse using the spacecraft charging model at a fixed value of $T_2 = 2.1$keV, which is around the typical electron temperature prior to the injection of the high energy particles at local midnight during periods of low solar activity [32]. It will be assumed that the ion density $n_{i_{1,2}}$ is equal to the electron density $n_{e_{1,2}}$ because the electron to proton density ratio is approximately 1 around local midnight during periods of low solar activity [32]. For simplicity, it will also be assumed that the ion temperature $T_{i_{1,2}}$ is equal to the electron temperature $T_{e_{1,2}}$, but it should be noted that the ion temperature in population 1 is typically several times greater than the electron temperature at local midnight. Including a hotter ion population does not significantly effect the value of α where the threshold occurs, however, as $T_{e_{1,2}}/T_{i_{1,2}} \to 0$, the curve shifts to the left such that lower values of T_{e1} would initiate a potential jump. The implications of this result will be discussed in the next section. The threshold occurs in the environment where the natural potential of the spacecraft changes from positive to negative. It follows a U-shape similar to that seen in Fig. 3. In this case, however, the minimum and maximum values of T_1 are offset from T_A and T^*. This makes sense because T_A and T^* are calculated using an environment that does not account for the ion contribution to charging.

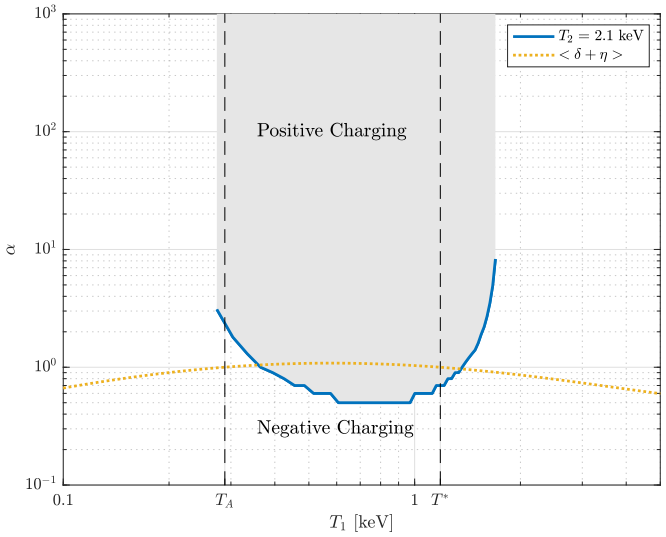

Fig. 4: Illustration of the threshold condition using a spacecraft charging model for a fixed $T_2 = 2.1$keV.

The key finding is that the charging threshold curve using the spacecraft charging model does not depend on the initial spacecraft potential ϕ_0. For any given ϕ_0, the threshold will follow a curve dependent on only T_1, T_2, and α. Additionally, the potential will converge to the same stable equilibria for a given environment regardless of ϕ_0.

IV. Results

A. Effect of the Electron Beam Current on the Charging Threshold

The addition of the electron beam even at very low currents (on the order of nA) causes the threshold curve for negative charging to increase by a factor of tens, hundreds, or more for the case where $T_A < T_1 < T^* < T_2$, meaning that in most typical GEO environments the spacecraft would not jump from an initial negative potential to a positive potential. As T_2 decreases, the threshold curve decreases, so there is most likely to be a jump to a positive potential with cool population 2 electrons and a very low electron beam current. In this paper, a beam current of 50μA at an energy of 20keV is used since this causes the electron beam to produce multiple equilibria in a single-Maxwellian environment [9].

The effect of a hot ion population was previously mentioned. As $T_{e_{1,2}}/T_{i_{1,2}} \to 0$, the threshold curve shifts to the left such that lower values of T_{e_1} would initiate a potential jump. This result is explained by the fact that the hot ion population would induce a significant positive current on the target that would dominate over the negative currents from the ambient electrons and the electron beam. Thus, the target potential is more likely to be positive. This is especially true with very low or negligible electron beam currents. However, with a 50μA beam current as being used in this research, the electron temperature must be significantly smaller than the ion temperature $T_{e_{1,2}}/T_{i_{1,2}} << 1$ in order to induce a jump to a positive potential. Based off of typical local midnight and local dawn temperatures [32], the scenario required to induce a jump to a positive potential is unrealistic and thus the effect of the ions is trivial. However, in worst-case scenarios [33], it is possible for the potential to jump to a positive value even while using the electron beam.

B. Active Charging with a Variable Electron Density Ratio

During a geomagnetic substorm, the population 2 particle density may increase as particles are injected into GEO. In this section, the electron and ion temperatures for populations 1 and 2 will be held constant as the electron density ratio α varies. The results will be discussed for a more mild plasma environment and for the worst case scenario as measured by the SCATHA mission [33].

1) Mild Plasma Environment: The mild plasma environment was chosen such that $T_A < T_1 < T^* < T_2$ for silver, which has $T_A = 0.3$keV and $T^* = 1.2$keV. Then, T_1 was selected to be 0.5105keV because this temperature closely corresponds to the electron temperature at GEO around local midnight before the injection of high-energy magnetosphere particles [32]. T_2 was selected to be 2.1keV to keep consistent with Figures 3 and 4. The electron beam current remains 50μA with an energy of 20keV.

Fig. 5 shows the result of active charging on the eclipsed target, neglecting the effects of the servicer spacecraft. Fig. 5a depicts the net current acting on the target as a function of the spacecraft electric potential ϕ and the electron density ratio α. When the current is greater than zero, the surface is colored green, and when the potential is less than zero, the surface is colored red. The equilibria occur when the current is equal to zero at the intersection of the green and red surfaces. The black points in the current-ϕ plane illustrates the 3 equilibrium potentials for an approximately single-Maxwellian plasma, $\alpha \to \infty$. The equilibrium potential is roughly the same for all values of $\alpha > 1$. However, for $\alpha < 1$, the equilibrium potential begins to increase by thousands of Volts. This can be more easily visualized in Fig. 5b, which depicts the charging of the target over time from 10 linearly spaced initial target potentials ranging from -1kV to -25kV. At each initial target potential, the environment is modified such that 50 linearly spaced values of α ranging from 0.1 to 2 are modeled over time. The blue lines show the cases where $\alpha < 1$ and the orange lines show the cases where $\alpha > 1$. The population 1 electron density n_1 is fixed at 0.2cm^{-3} while $n_2 = \alpha/n_1$. The ion densities are equal to the electron densities.

On the black curve in Fig. 5a, the most and least negative equilibria are stable, while the middle equilibrium is unstable. The most negative equilibrium at -20kV corresponds to the energy of the electron beam. This is the case where the electron beam is initially unable to reach the target due to the target being severely negatively charged. This causes the target to converge to the most negative potential possible for a given electron beam energy. The least negative equilibria is the caused by the impact of the electron beam and the resulting secondary and backscattered electron emission. The target potential may jump between these equilibria but will never converge to the unstable middle equilibrium.

It can also be observed in both Fig. 5a and 5b that as $\alpha \to \infty$, the potential converges to 1 of the 2 stable equilibria

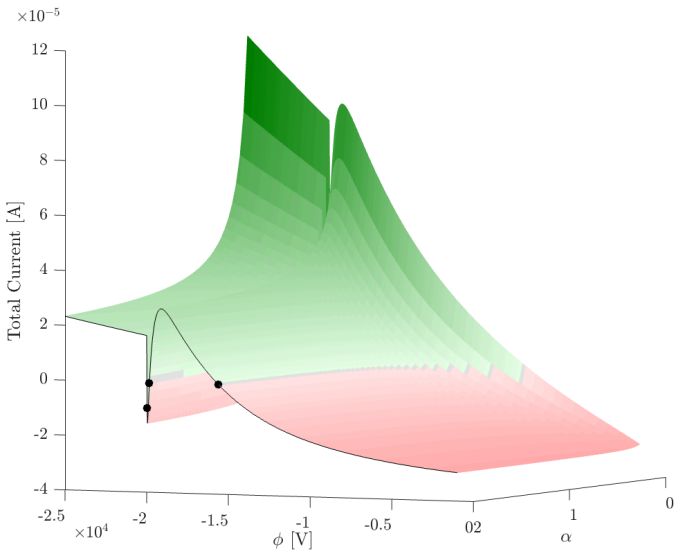

(a) Total current acting on the target as a function of the spacecraft electric potential and the electron density ratio.

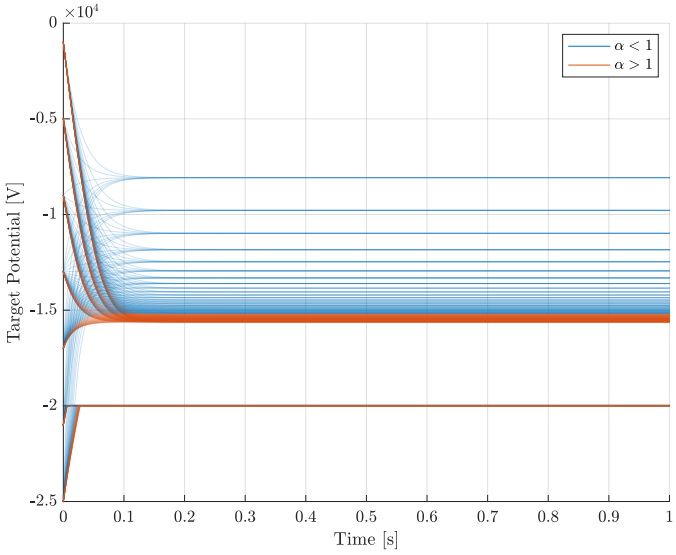

(b) Target potential over time for various initial potentials and a range of electron density ratios.

Fig. 5: Effect of electron beam on target potential without accounting for the charging of the servicer spacecraft.

denoted by the black curve in Fig. 5a. This result indicates that charging is most predictable when $n_1 > n_2$. When $n_1 < n_2$, the target potential may jump suddenly between hundreds or even thousands of volts when the environment is perturbed. Since the environment in a bi-Maxwellian plasma may have a significant and unpredictable impact on the equilibrium potential of the target in an eclipse, the electrostatic tractor would operate most successfully when n_2 is negligible, which would be most likely to occur in quiet periods long past local dawn hours and before local midnight.

When including the servicer in the charging simulation, the situation will be modeled such that the servicer is in full sun and is itself eclipsing the target. Then, the photoelectric current affects the servicer but does not affect the target. As a result, the servicer is initially charged positively, while the target is initially charged negatively.

Fig. 6 shows the target potential over time from 10 linearly spaced initial target potentials ranging from -1kV to -25kV. At each initial target potential, the environment is modified such that 50 linearly spaced values of α ranging from 0.1 to 10 are modeled over time, as opposed to 0.1 to 2 for Fig. 5b. The blue lines show the cases where $\alpha < 1$ and the orange lines show the cases where $\alpha > 1$. At each new value of α, the servicer equilibrium potential is recalculated and used as the initial servicer potential. Similarly to the case without accounting for the charging of the servicer, the target converges to 1 of 2 stable equilibria as $\alpha \to \infty$. However, the servicer causes the target to converge to a particular potential at higher values of α than for the case without the servicer. It can be observed that for $\alpha > 1$, many of the less negative initial target potentials begin to decrease before changing direction and increasing, ultimately converging to a negative potential that is, in some cases, more positive than the initial potential. This is the effect of the coupling of the environment and the electron beam. Without the electron beam, $\alpha > 1$ converge to a slightly positive potential because the α charging threshold for this environment is less than 1. The electron beam initiates negative charging, but the currents related to the environment initiate positive charging. The positive charging of the servicer over time as it releases electrons from the electron beam weakens the impact of the electron beam on the target as some electrons are attracted back to the servicer. Therefore, the initial negative charging of the target is reversed as a result of the positive charging from the environment coupled with the attraction of the electrons to the positively charged servicer. The most negative equilibrium potential in this case also no

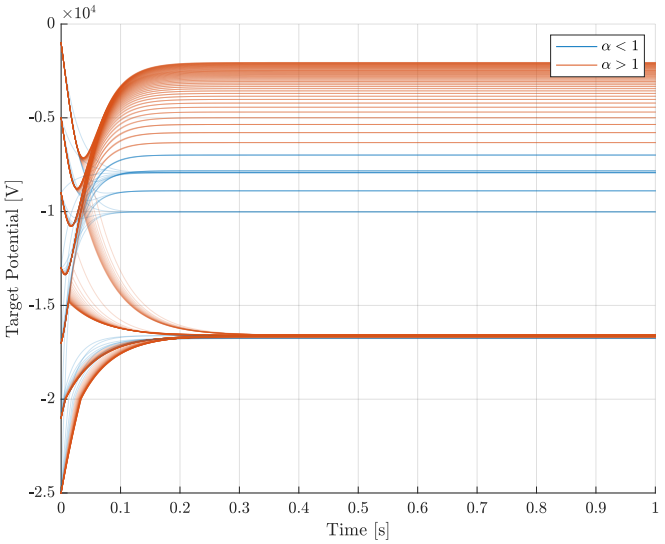

Fig. 6: Target potential over time for various initial potentials and a range of electron density ratios including the effect of the servicer on charging.

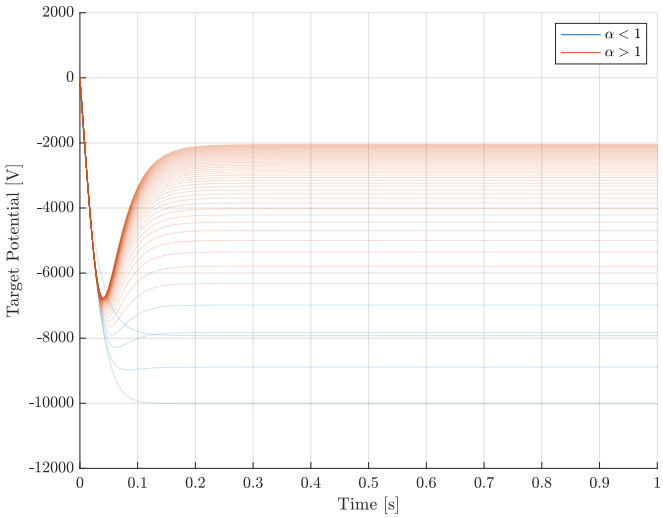

Fig. 7: Charging of the target over time starting from the natural potential.

longer corresponds the electron beam energy. This is again due to the positive influence of the environment on the charging of the target and the weakening of the electron beam due to the positive charging of the servicer.

Fig. 7 shows the charging of the target over time starting from the natural potentials of both the target and the servicer at each value of α. Again, $\alpha > 1$ are shown in orange and $\alpha < 1$ are shown in blue. The pattern is consistent with that seen in Fig. 6 for less negative initial target potentials. The equilibrium potential converges to a particular value as $\alpha \to \infty$.

The key takeaway is that including the charging of the servicer in the simulation increases the value of α required to converge to a particular equilibrium value. As previously stated, the electrostatic tractor would be most effective and easiest to control when $n_1 \gg n_2$.

2) SCATHA Worst-Case Environment: The worst-case bi-Maxwellian environment was measured during the SCATHA mission on April 24, 1978 [33]. The parallel measurements can be seen in Table I. In this research, the ion and electron values for T_1, T_2, and n_1 will be used, while $n_2 = \alpha/n_1$ as α varies.

TABLE I: SCATHA Worst-Case Environment [33]

Particle Type	Parameter			
	$\mathbf{T_1}$ [keV]	$\mathbf{T_2}$ [keV]	$\mathbf{n_1}$ [cm^{-3}]	$\mathbf{n_2}$ [cm^{-3}]
Electron	0.4	24	0.2	0.6
Ion	0.3	26	1.6	0.6

Fig. 8 shows the result of active charging on the eclipsed target, neglecting the effects of the servicer. Fig. 8a depicts the net current acting on the target as a function of the spacecraft electric potential ϕ and the electron density ratio α. When the current is greater than zero, the surface is colored green, and when the potential is less than zero, the surface is colored red. The equilibria occur when the current is equal to zero at the intersection of the green and red surfaces. Unlike in Fig. 5a, the surface in Fig. 8a only crosses zero once. This indicates that there is only 1 negative, stable equilibrium potential for each value of α where a zero-crossing occurs. For values of α where the current always remains above zero, the potential will jump to a positive potential. This is clear in Fig. 8b, which depicts the charging of the target over time from 10 linearly spaced initial target potentials ranging from -1kV to -25kV. At each initial target potential, the environment is modified such that 50 linearly spaced values of α ranging from 0.1 to 10 are modeled over time. The blue lines show the cases where $\alpha < 1$ and the orange lines show the cases where $\alpha > 1$. For several values of $\alpha < 0$, the target potential converges to a positive potential. This is problematic for the electrostatic tractor concept because to pull the target into a graveyard orbit, the target must be charged negatively while the servicer charges positively due to electron beam emission. A stronger electron beam current could be used to prevent positive charging in this environment. Similarly to the results for the mild environment, the equilibrium potential eventually converges to a particular value as $\alpha \to \infty$. Again, the electrostatic tractor would be most effective when $n_1 \gg n_2$, and positive charging would also be avoided in this situation.

The charging behavior due to including the servicer has the same effect for the SCATHA worst-case environment as it did for the mild environment.

C. Active Charging with Variable Population 2 Electron Temperature

During a geomagnetic substorm, the population 2 temperature may increase as particles are excited during the snap-back of the magnetotail. The effect of a varying T_2 is modeled in 9. The plots in the figure show the total current acting on the target spacecraft as a function of the spacecraft potential ϕ and the population 2 electron temperature T_2, where T_2 ranges from T^* to 24keV, the worst case environment as measured by SCATHA. The population 2 ion temperature also varies from T^* to 26keV, which is, again, the worst case environment measured by SCATHA. The population 1 electron temperature and ion temperature are both 0.5105keV to keep consistent with typical quiet environments. Electron density ratios for three different environments are represented: $\alpha = 0.1$, 1, and 2.

The green colored surface represents areas when the current is greater than zero, while the red colored surface shows where the current is below zero. The equilibrium potentials occur at the intersection of the green and red areas, where the surface crosses zero current. In Fig. 9b and 9c, where $\alpha \geq 1$, there are 3 equilibrium potentials for each value of T_2. In Fig. 9a, where $\alpha < 1$, there is only 1 equilibrium potential for each T_2. While this result is expected from previous data, Fig. 9 helps visualize the effect of $\alpha \to 0$, which could not be easily observed in other figures.

It is apparent from Fig. 9 that for $\alpha \geq 1$, varying T_2 does not have a significant effect on the equilibrium potential. Except for values of T_2 that are close to T^*, the equilibrium potential is constant. When T_2 is close to T^*, the equilibrium potential decreases slightly. However, when $\alpha < 1$, variations of T_2 cause the equilibrium potential to change at every value of T_2.

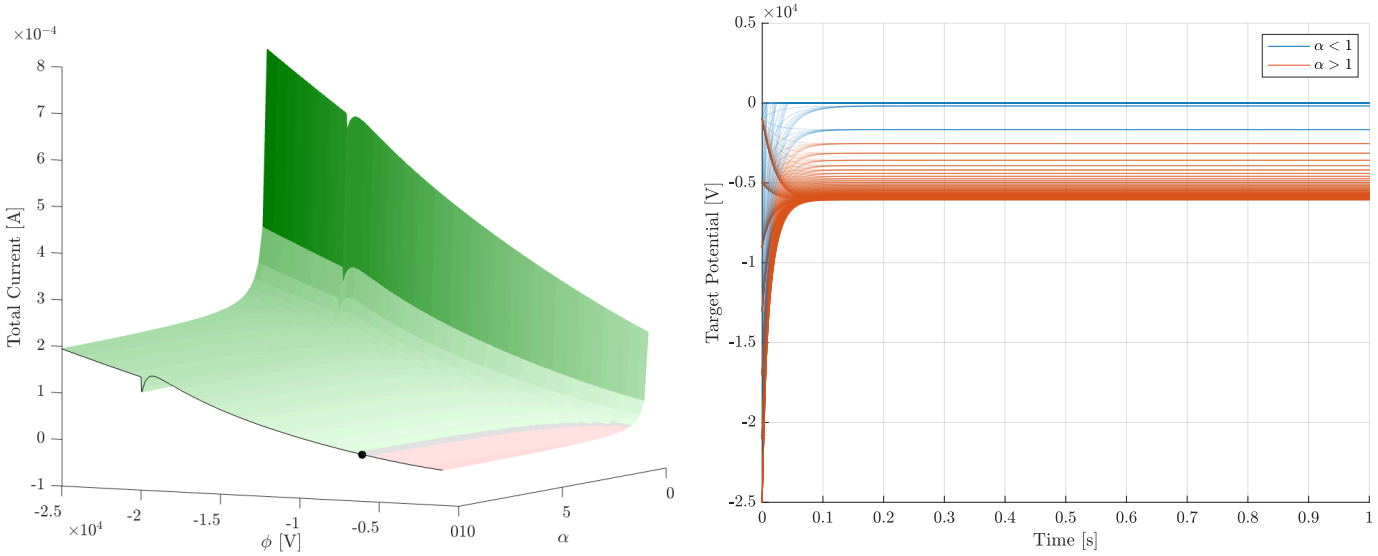

(a) Total current acting on the target as a function of the spacecraft electric potential and the electron density ratio.

(b) Target potential over time for various initial potentials and a range of electron density ratios.

Fig. 8: Effect of electron beam on target potential without accounting for the charging of the servicer spacecraft.

This result is intuitive because as n_2 increases (thus decreasing α), T_2 will have a stronger effect on the charging of the target.

These results ultimately perpetuate the conclusion that the electrostatic tractor would be most effective in an environment where $n_1 \gg n_2$. The other interesting result is that as $T_2 \rightarrow T^*$, the equilibrium potential becomes increasingly mutable.

V. Conclusion

This paper investigates the effectiveness of the electrostatic tractor concept in a bi-Maxwellian space environment. In this analysis, an electron beam is assumed to be mounted onto a servicer spacecraft. The electron beam is directed at a target spacecraft, resulting in electron beam emission from the servicer and electron beam impact on the target. Then, the servicer is charged positively and the target should be charged negatively to initiate an attractive electrostatic force between the spacecraft, which would allow the servicer to pull the target into a graveyard orbit.

The threshold for negative charging in a bi-Maxwellian plasma is found to not be dependent on the initial spacecraft potential. For a particular combination of temperatures, the spacecraft will jump either to a positive or negative potential at the same electron density ratio $\alpha = n_1/n_2$. Overall, the threshold is dependent only on T_1, T_2, and α. When the electron beam is in use, a jump to a positive potential is most likely when the electron beam current is very low and the population 2 electron temperature T_2 is also low. Ions may also initiate a jump to a positive potential by shifting the threshold curve to the left such that the potential jump occurs at lower population 1 temperatures T_1.

The overarching conclusion of this research is that the elecrostatic tractor is most effective in environments where $n_1 \gg n_2$. This is because as $\alpha \rightarrow \infty$, the equilibrium potential of the target will always converge to a particular value such that perturbations in the environment would have minimal effect on the target potential. At different values of $\alpha \rightarrow 0$, the equilibrium potentials are hundreds or thousands of Volts apart. A slight perturbation in the environment when α is small would cause a drastic change in potential of the target. In extreme environments, a perturbation when α is small may even cause the potential to jump to a positive value, making the electrostatic tractor completely ineffectual.

Variations in the population 2 electron temperature T_2 have minimal effect on the target equilibrium potential except where α is small. Perturbations in T_2 also have a stronger effect when T_2 is very close to T^*. Therefore, the electrostatic tractor is more predictable when the electrons in population 2 are hot. This environment also helps avoid possible jumps to a positive potential.

Future research will model the electrostatic forces and torques that result from the potentials generated in a bi-Maxwellian plasma. Photoelectron emission on the the target will also be accounted for, and different levels of sun exposure will be modeled. Active charging using alternate velocity distribution functions will also be considered, including the kappa function and a combination of Maxwellian and kappa distributions.

Acknowledgment

The authors would like to thank Julian Hammerl for his spacecraft charging model and Kaylee Champion for her assistance acquiring NASCAP material properties. This work was supported by the U.S. Air Force Office of Scientific Research under grant FA9550-21-S-001

References

[1] H. Schaub, L. E. Jaspera, P. V. Anderson, and D. S. McKnight, "Cost and risk assessment for spacecraft operation decisions caused by the space debris environment," *Acta Astronautica*, 2015.

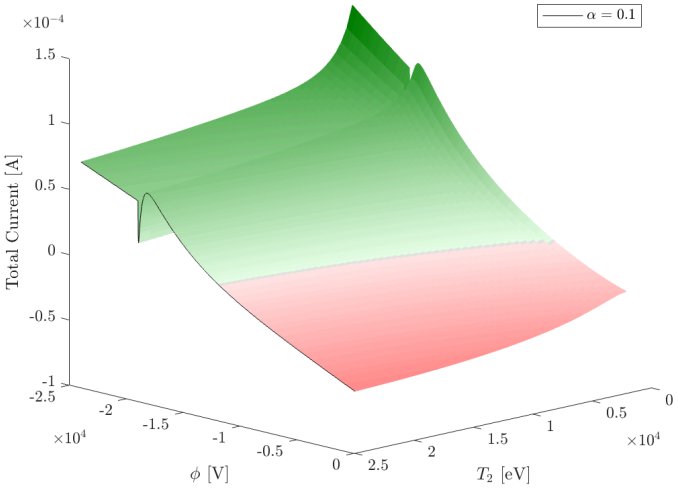

(a) Total current acting on the target as a function of ϕ and T_2 for $\alpha = 0.1$.

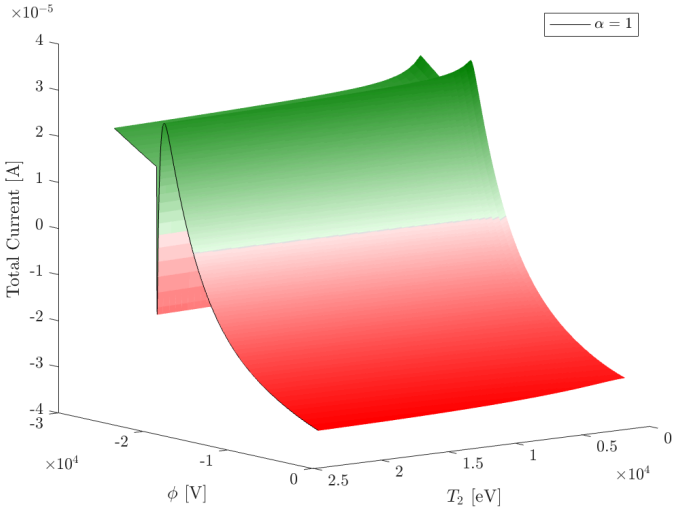

(b) Total current acting on the target as a function of ϕ and T_2 for $\alpha = 1$.

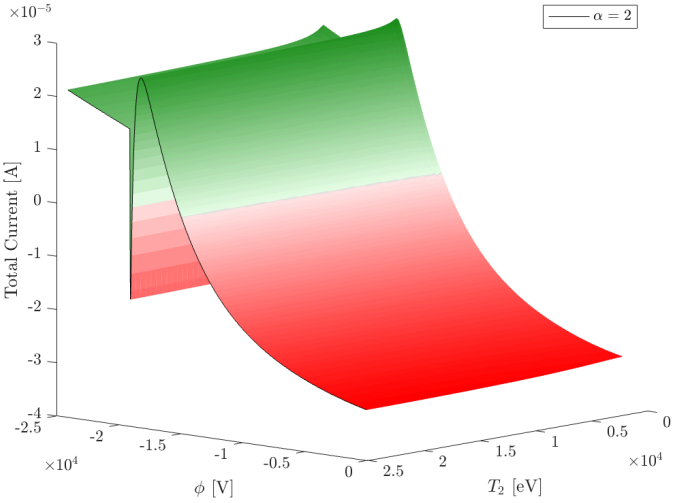

(c) Total current acting on the target as a function of ϕ and T_2 for $\alpha = 2$.

Fig. 9: Total current acting on the target as a function of ϕ and T_2 for $\alpha = 0.1$, 1, and 2.

[2] D. L. Oltrogge, S. Alfano, C. Law, A. Cacioni, and T. S. Kelso, "A comprehensive assessment of collision likelihood in geosynchronous earth orbit," *Acta Astronautica*, vol. 147, pp. 316–345, 2018.

[3] H. Zhang, Z. Li, W. Wang, Y. Zhang, and H. Wang, "Geostationary orbital debris collision hazard after a collision," *Aerospace*, vol. 9, p. 258, 2022.

[4] P. Papushev, Y. Karavaev, and M. Mishina, "Investigations of the evolution of optical characteristics and dynamics of proper rotation of uncontrolled geostationary artificial satellites," *Advances in Space Research*, vol. 43, pp. 1416–1422, 2009.

[5] Y. Karavaev, R.M.Kopyatkevich, M. Mishina, G. Mishin, P. Papushev, and P. Shaburov, "The dynamic properties of rotation and optical characteristics of space debris at geostationary orbit," *Advances in the Astronautical Sciences*, p. 1457–1466, 2004.

[6] E. H. Trevor Bennett, Daan Stevenson and H. Schaub, "Prospects and challenges of touchless electrostatic detumbling of small bodies," *Advances in Space Research*, vol. 56, pp. 557–568, 2015.

[7] H. Schaub and J. D. F. Moorer, "Geosynchronous large debris reorbiter: Challenges and prospects," *The Journal of Astronautical Sciences*, vol. 59, pp. 161–176, 2012.

[8] K. Champion and H. Schaub, "Electrostatic potential shielding in representative cislunar regions," *IEEE TRANSACTIONS ON PLASMA SCIENCE*, vol. 51, 2023.

[9] J. Hammerl and H. Schaub, "Coupled spacecraft charging due to continuous electron beam emission and impact," *Journal of Spacecraft and Rockets*, under review.

[10] E. A. Hogan and H. Schaub, "Impacts of hot space plasma and ion beam emission on electrostatic tractor performance," *IEEE TRANSACTIONS ON PLASMA SCIENCE*, vol. 43, 2015.

[11] M. D. Montgomery, S. J. Bame, and A. J. Hundhausen, "Solar wind electrons: Vela 4 measurements," *Journal of Geophysical Research*, 1968.

[12] W. C. Feldman, J. R. Asbridge, S. J. Bame, M. D. Montgomery, and S. P. Gary, "Solar wind electrons," *Journal of Geophysical Research*, 1975.

[13] W. G. Pilipp, H. Miggenrieder, M. D. Montgomery, K. H. Mühlhäuser, and H. R. amd R. Schwenn, "Characteristics of electron velocity distribution functions in the solar wind derived from the helios plasma experiment," *Journal of Geophysical Research*, 1987.

[14] V. P. Milan Maksimovic and P. Riley, "Ulysses electron distributions fitted with kappa functions," *Journal of Geophysical Research*, 1997.

[15] I. Zouganelis, "Measuring suprathermal electron parameters in space plasmas: Implementation of the quasi-thermal noise spectroscopy with kappa distributions using in situ ulysses/urap radio measurements in the solar wind," *Journal of Geophysical Research*, 2008.

[16] V. Pierrard and M. Lazar, "Kappa distributions: Theory and applications in space plasmas," *Solar Physics*, 2010.

[17] R. Perez, *Wireless Communications Design Handbook*. Elsevier, 1998, vol. 1.

[18] G. D. R. Chao-Song Huang, *Multiscale Coupling of Sun-Earth Processes*. Elsevier, 2005.

[19] J. G. Laframboise, R. Godard, and M. Kamitsuma, "Multiple floating potentials, threshold temperature effects, and barrier effects in high voltage charging of exposed surfaces on spacecraft," in *Proceedings of International Symposium on Spacecraft Materials in Space Environment*, 1982.

[20] S. T. Lai, "Theory and observation of triple-root jump in spacecraft charging," *Journal of Geophysical Research*, vol. 96, 1991.

[21] S. T. Lai and D. J. Della-Rose, "Spacecraft charging at geosynchronous altitudes: New evidence of existence of critical temperature," *Journal of Spacecraft and Rockets*, vol. 38, pp. 922–928, 2001.

[22] S. Lai and M. Tautz, "High-level spacecraft charging in eclipse at geosynchronous altitudes: A statistical study," *Journal of Geophysical Research*, vol. 111, 2006.

[23] S. T. Lai, *Fundamentals of Spacecraft Charging*. Princeton University Press, 2012.

[24] J. Huang, G. Liu, and L. Jiang, "Threshold for spacecraft charging in double-maxwellian plasma," *Journal of Geophysical Research: Space Physics*, vol. 120, p. 6301–6308, 2015.

[25] N. L. Sanders and G. T. Inouye, "Secondary emission effectson spacecraft charging: Energy distribution consideration," *Spacecraft Charging Technology—1978*, 1979.

[26] S. M. Prokopenko and J. G. L. Laframboise, "High voltage differential charging of geostationary spacecraft," *Journal of Geophysical Research*, vol. 85, 1980.

[27] S. Ali, N. Rubab, K. Nawaz, and S. Sawar, "A comparative study of spacecraft charging onset at geosynchronous altitudes: A nonextensive particle approach," *Journal of Geophysical Research: Space Physics*, 2020.
[28] V. Davis, B. Gardner, and M. Mandell, "Nascap-2k version 4.3 users manual," *Leidos Holdings San Diego, CA, USA, Tech. Rep. AFRL-RVPS-TR-2017-0002*, 2016.
[29] E. W. Jr., "he equilibrium electric potential of a body in the upper atmosphere and in inter-planetary space," Ph.D. dissertation, George Washington University, 1965.
[30] C. Nam, N. Hershkowitz, M. H. Cho, T. Intrator, , and D. Diebold, "Multiple valued floating potentials of langmuir probes," *Journal of Applied Physics*, vol. 63, pp. 5674–5677, 1988.
[31] J. Huang, G. Liu, and L. Jiang, "Theory of spacecraft potential jump 10.1002/2015ja021820 in geosynchronous plasma," *Journal of Geophysical Research: Space Physics*, 2015.
[32] M. H. Denton, M. F. Thomsen, H. Korth, S. Lynch, J. C. Zhang, and M. W. Liemohn, "Bulk plasma properties at geosynchronous orbit," *Journal of Geophysical Research: Space Physics*, 2005.
[33] E. Mullen, M. Gussenhoven, and H. Garrett, "A "worst case" spacecraft environment as observed by scatha on 24 april 1979," *Environmental Research Papers*, no. 751, 1981.